Acta Materialia 244 (2023) 118551

Contents lists available at ScienceDirect

Acta Materialia

journal homepage: www.elsevier.com/locate/actamat

Anelastic-like nature of the rejuvenation of metallic glasses by cryogenic thermal cycling

Miguel B. Costa [a], Juan J. Londoño [b,c], Andreas Blatter [b], Avinash Hariharan [d], Annett Gebert [d], Michael A. Carpenter [e], A. Lindsay Greer [a,f,*]

[a] Department of Materials Science and Metallurgy, University of Cambridge, Cambridge CB3 0FS, United Kingdom
[b] Research and Development Department, PX Services, La Chaux-de-Fonds 2300, Switzerland
[c] Department of Materials Science, Montanuniversität Leoben, Leoben 8700, Austria
[d] Institute for Complex Materials, Leibniz Institute for Solid State and Materials Research, Dresden (IFW Dresden), D-01069 Dresden, Germany
[e] Department of Earth Sciences, University of Cambridge, Cambridge CB2 3EQ, United Kingdom
[f] WPI Advanced Institute for Materials Research, Tohoku University, Sendai 980-8577, Japan

ARTICLE INFO

Keywords:
Bulk metallic glasses
Mechanical properties
Structural relaxation
Thermal cycling
Anelasticity

ABSTRACT

Cryogenic thermal cycling (CTC) is an effective treatment for improving the room-temperature plasticity and toughness in metallic glasses. Despite considerable attention to characterizing the effects of CTC, they remain poorly understood. A prominent example is that, contrary to expectation, the stored energy in a metallic glass first rises, and then decreases, as CTC progresses. In this work, CTC is applied to bulk metallic glasses based on Pd, Pt, Ti, or Zr. The effects on calorimetric and mechanical properties are evaluated. Critically, CTC-induced effects, at whatever stage, are found to decay over about one week at room temperature after CTC, returning the properties to those of the as-cast glass. A model is proposed for CTC-induced effects, treating them as analogous to the accumulation of anelastic strain. The implications for analysis of existing data, and for future research on CTC effects, are highlighted.

1. Introduction

Metallic glasses (MGs) attract interest across several fields: they possess distinct functional properties [1], and have broadened our understanding of the nature and formation of the glassy state [2]. New glasses, still being found, broaden the portfolio of materials for practical applications. MGs have found a wide range of uses [3–5]. Most notably Fe-based MGs and glass-crystal nanocomposites derived from them, are excellent soft-magnetic materials [6,7]. On the other hand, intrinsic lack of ductility and tendency to embrittlement by structural relaxation [8,9] hinder wide application of MGs as structural materials [10].

A countermeasure to embrittlement is to induce structural changes to less relaxed (i.e. *rejuvenated*) states of higher energy. Several thermo-mechanical processing techniques have been used to achieve this [11]. Processes within the elastic limit [12] (*elastostatic loading* and *cryogenic thermal cycling*, CTC) are of particular interest in probing the microscopic mechanisms acting in MGs exposed to external stimuli (mechanical and thermal). CTC is attractive: easy to apply to complex shapes, giving negligible shape change, and efficient at changing the state to one of higher energy [13,14]. The effects of CTC include several signs of rejuvenation: increased volume of the soft spots and *shear-transformation zones* (STZs) [15,16]; reduced relaxation times [17]; reduced yield stress, hardness [18,19] and density [16]; increased plasticity [20] and toughness [21,22]. The effects depend on the composition [23,24] and initial state of the glass [13,25], and on processing parameters [16].

Mappings of local properties before and after processing by CTC indicate that MGs are more heterogeneous when rejuvenated [26]. Heterogeneity in MGs is likely a key factor enabling rejuvenation by CTC [13,27]. Molecular-dynamics simulations of a MG show that heterogeneity of thermal expansion, giving non-affine deformations, can induce structural change [28]. Model glasses formed at higher cooling rates are more heterogeneous, and are more amenable to rejuvenation by CTC. The lack of rejuvenation by CTC in well annealed MGs [13,25], is explained by the reduction in structural heterogeneity caused by the annealing.

It is commonly observed that as CTC progresses, the stored energy in a MG first increases, reaches a sharp maximum, and then decreases. This non-monotonic behaviour is unexpected, and has not been explained. In

* Corresponding author.
E-mail address: alg13@cam.ac.uk (A.L. Greer).

https://doi.org/10.1016/j.actamat.2022.118551
Received 23 May 2022; Received in revised form 23 November 2022; Accepted 23 November 2022
Available online 24 November 2022

the present work, this behaviour is explored for four compositions, in detail for two. The $Pd_{43}Cu_{27}Ni_{10}P_{20}$ BMG is an example from the metal-metalloid family for which it has been questioned whether CTC has any significant effect [29]. The metal-metal $Ti_{40}Zr_{10}Cu_{34}Pd_{14}Sn_2$ BMG permits comparison with published results on similar compositions [16,18]. Non-monotonic behaviour is confirmed in these BMGs, both for stored energy and dispersion of microhardness. The non-monotonic behaviour, and associated memory effects, are considered to have essentially the same structural basis as anelasticity.

2. Experimental methods

Alloys were prepared from elements of 3–4N purity. Ingots of $Pd_{43}Cu_{27}Ni_{10}P_{20}$ (at.%) were prepared, and then re-melted in a vacuum induction furnace, and tilt-cast into 3-mm-thick plates. In contrast to common laboratory-scale processing of similar alloys, no fluxing agent was used. An ingot of $Ti_{40}Zr_{10}Cu_{34}Pd_{14}Sn_2$ (at.%) was prepared by arc-melting under a high-purity argon atmosphere, then re-melted and suction-cast into a water-cooled copper mould to produce a 3-mm-thick plate. No crystallinity was detected in any of the as-cast plates using standard X-ray diffractometry (CoKα radiation). These Pd-based and Ti-based BMGs are the focus of the present study. Three additional metallic glasses ($Zr_{52.5}Ti_5Cu_{17.9}Ni_{14.6}Al_{10}$, $Pt_{57.5}Cu_{14.7}Ni_{5.3}P_{22.5}$, and $Pd_{43}Cu_{27}Ni_{10}P_{20}$) were suction-cast into 3-mm-diameter rods in a water-cooled copper mould; results on these MGs are reported in Supplementary Material. For a given composition, the suction-casting in the present work gives faster cooling than tilt-casting.

For CTC treatments, BMG samples were immersed in liquid nitrogen for 1 min, then held in a room-temperature (RT) airflow (from a hair-dryer) for 1 min. Samples were treated up to 200 thermal cycles (TCs).

Differential scanning calorimetry (DSC) was carried out using a Q2000 DSC (TA Instruments). A sapphire sample was used to calibrate the measurement of specific heat (C_p). The DSC signal can be affected by contamination of the sample surfaces. Good reproducibility was achieved by cleaning the DSC samples in two steps: ultrasonic cleaning in an acetone bath, then in an ethanol bath. The chosen sample mass of 15–20 mg gave a good signal-to-noise ratio in the DSC traces, without smearing due to temperature differences within the samples.

After the first DSC heating run on each sample, the sample was crystallized, and a second run on the now-crystalline sample, with the same heating rate and temperature range as the first run, was used to generate the baseline for subtraction from the signal in the first run. The heat of relaxation, ΔH_{rel}, was then calculated as the area between the baseline-subtracted curves and a straight-line extrapolation of the low-temperature portion of the DSC trace, from the onset of relaxation to the onset of the glass transition [30]. For each treated state, 3–5 samples were evaluated for statistical accuracy. For consistency of the results, the ΔH_{rel} values (§3.1) were measured within 24–48 h of carrying out each thermal treatment.

For the distinct BMGs, different protocols were adopted to crystallize the samples at the end of the first run. The Pd-based and Pt-based BMG samples were heated at 20 K min^{-1} from RT to 823 K (into the liquid state), then cooled to 723 K (below the crystallization peak on cooling) at 5 K min^{-1}, thus ensuring the sample fully crystallizes during cooling (as further confirmed by DSC). The Ti-based and Zr-based BMG samples were heated at 20 K min^{-1} from RT to 823 K (above the crystallization onset temperature, but no further, because of instrument limitations) and then held for five minutes to fully crystallize the sample.

Vickers microhardness mapping was carried out using an automated hardness tester (Q30 A+, *Qness*). Microhardness (H_V) was measured at 0.49 N load with a 10 s loading time. To avoid potential surface effects due to CTC (detected to a depth of ~10 nm [23]), the samples were ground with 1200 grit SiC papers for 30 seconds, followed by polishing with 2500 grit SiC paper. Subsequent polishing with 1-μm diamond paste gave a surface quality permitting sharp focus in optical images. According to the ASTM E384-17 standard, the centre-to-centre distance between indents should be at least 2.5 times the length of the indentation diagonals to avoid interference. The distance between neighbouring indentations was chosen to be at least 20 μm (the measured indent diagonals in this work were 3.7–4 μm). A minimum of 80 indents were made to characterize each condition. Derived directly from indent diagonals, the hardness values in the present work follow common practice in comparing samples, and allow a reliable differentiation between samples of a given composition in different states. It is noted that the apparent hardness may be affected by indentation pile-up, the extent of which varies with the structural state of the MG. Such effects have been studied [31] for structural states over a range, as characterized by a hardness range of >20%, that is some ten times that in the present work. For a valid comparison of the results, microhardness measurements were made (24 ± 2) h after each CTC treatment.

Resonant ultrasound spectroscopy (RUS) was performed on a $Pd_{43}Cu_{27}Ni_{10}P_{20}$ cuboid sample (4.394 × 3.308 × 2.392 mm^3) for determination of the elastic constants at RT in the as-cast and rejuvenated states. The approach used for determining the absolute values of the elastic moduli were the same as those described by McKnight et al. [32]. This involved matching of observed and calculated resonance frequencies using standard software [33]. The electronics used for collection of primary spectra have been described by Balakirev et al. [34]. For consistency of the assessments, a single sample was used for all the conditions tested. This sample was polished beforehand in a lapping rig to ensure the perpendicularity and parallelism of its faces (within 0.5°). For each condition, six resonance spectra were collected (with different contact configurations in the apparatus) in the frequency range 0.15–1.5 MHz. Each spectrum contained at least 5 × 10^5 data points. Frequencies were determined for the first 45 resonance peaks by fitting each with an asymmetric Lorentzian function [35]. For each sample tested, the data were fitted with two models: one taking the material to be isotropic, the other taking it to be uniaxial anisotropic. The computed elastic constants in both models match very well, confirming that the BMG is macroscopically isotropic for all conditions tested. A list of criteria for what constitutes a good fit between observed and calculated resonance frequencies has been given by Migliori and Maynard [36] but, in general, the fit is considered to be good when the root-mean-square (RMS) error is <0.5 %. In the present work, the RMS error was <0.3 % for all states tested, representing an excellent fit. The RUS spectra were acquired within 24 h following CTC.

3. Results

3.1. Increase in stored energy following cryogenic thermal cycling

When an as-cast MG is heated at a rate lower than the cooling rate at which it was formed, there is a heat release as the glass transition is approached. This heat of relaxation, ΔH_{rel} (shaded areas in Fig. 1) provides the most straightforward quantification of the relative enthalpy of the MG, and can be used to derive its fictive temperature [37]. DSC runs were carried out on Ti-based and tilt-cast Pd-based BMG samples, as-cast, and after different numbers of cryogenic TCs (selected results in Fig. 1). CTC induces no differences (within ±2 K) in glass-transition temperature T_g, or crystallization onset temperature T_x.

The exotherms in Fig. 1 define a relaxation spectrum for each glass. The shapes of the spectra for each glass are qualitatively the same as those in the literature on identical or similar compositions [38,39]. The shapes of the spectra are discussed in Supplementary Material, where Fig. S1 shows additional DSC data: for the suction-cast Pd-based glass cast at higher cooling rate, for a Pt-based BMG and for a Zr-based BMG.

To verify reproducibility for the tilt-cast Pd-based BMG, changes in ΔH_{rel} with CTC were measured for two batches of material; the results are consistent (Fig. 2a). A similar evolution of ΔH_{rel} with CTC was reported for other MGs [13,18,22]. As examined more closely in the present work (increments of 20 cycles up to 200 cycles), ΔH_{rel} first increases to a peak of 585 J mol^{-1}, i.e. an energy increase of 208 J mol^{-1}

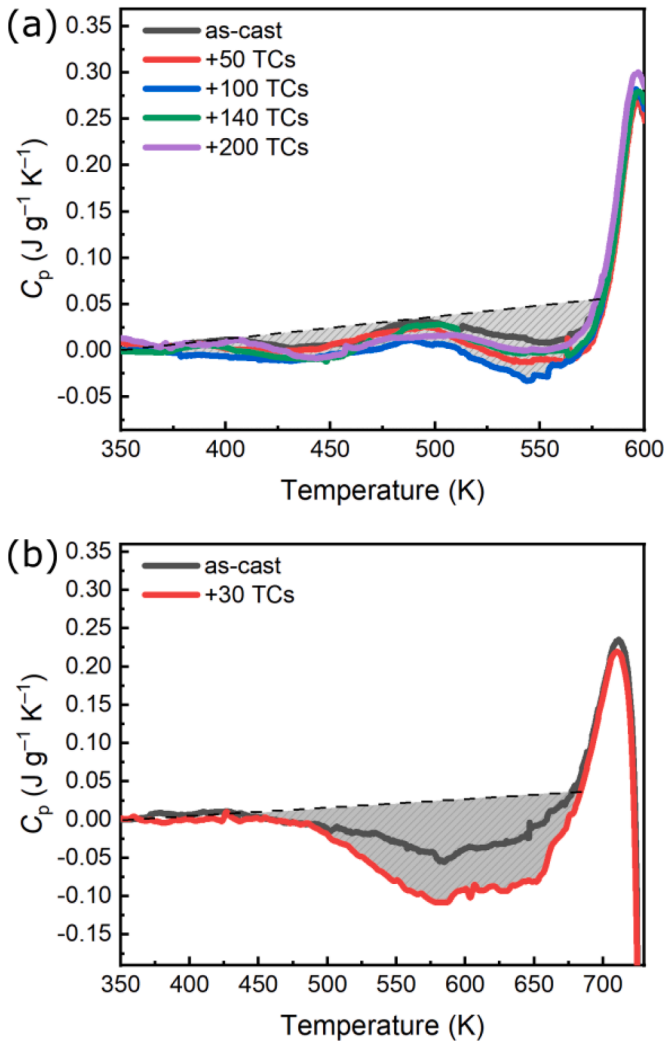

Fig. 1. Differential scanning calorimetry (DSC), heating at 20 K min^{-1}, of (a) tilt-cast $Pd_{43}Cu_{27}Ni_{10}P_{20}$ and (b) $Ti_{40}Zr_{10}Cu_{34}Pd_{14}Sn_2$ BMG samples in the as-cast state and following cryogenic thermal cycling. Structural relaxation during heating is evident as an exotherm (shaded area) before the glass transition. The traces shown are after baseline subtraction (§2). The enthalpy of relaxation (ΔH_{rel}) is measured relative to an extrapolation (dashed line) of the pre-exotherm specific heat (C_p).

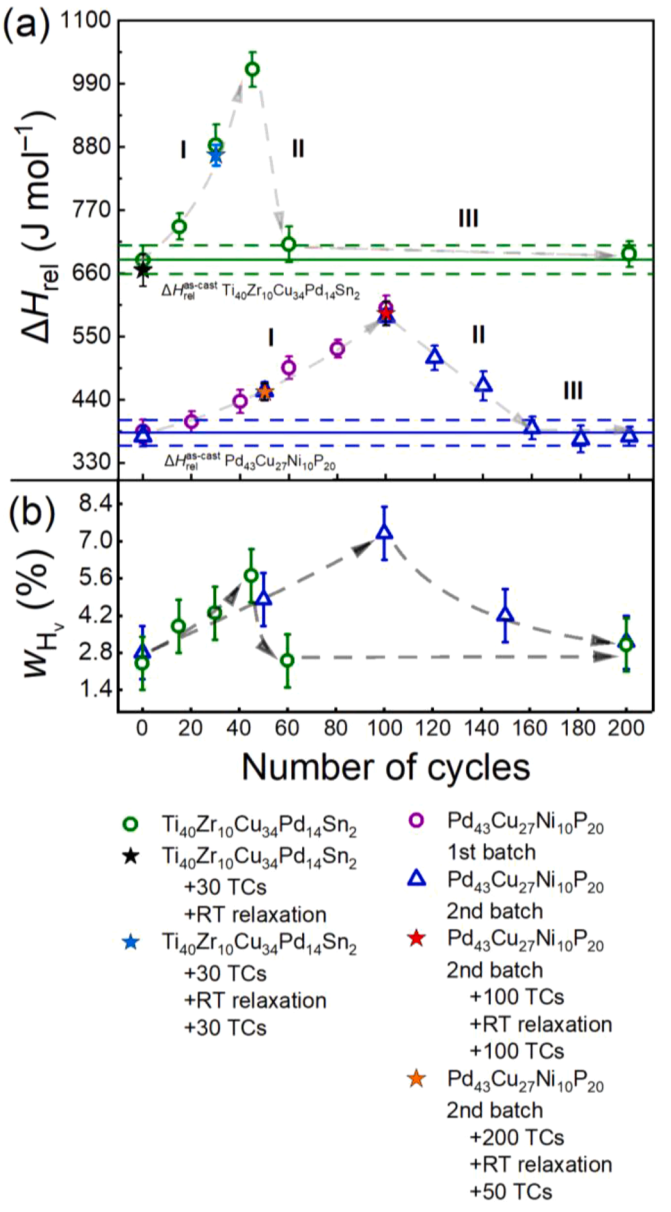

Fig. 2. Effects of CTC on $Ti_{40}Zr_{10}Cu_{34}Pd_{14}Sn_2$ and tilt-cast $Pd_{43}Cu_{27}Ni_{10}P_{20}$ BMGs. (a) The heat of relaxation ΔH_{rel}, as determined from the thermograms, evolves in three regimes, showing rejuvenation up to 45 or 100 TCs, relaxation at 45–60 or 100–160 TCs, and a steady state after 60 or 160 TCs in the Ti-based and tilt-cast Pd-based BMGs, respectively. The horizontal solid line in each case indicates the average ΔH_{rel} of the as-cast state; the dashed lines show ±1 SD from the average. The holding times at RT to achieve relaxation were 1.5 months- (b) The width of the distributions of microhardness values (w_{Hv}) (Fig. 3).

relative to the as-cast state; it then decreases to approximately the value for the as-cast state (377 J mol^{-1}). Further CTC does not significantly change ΔH_{rel}.

For the Ti-based BMG (Fig. 2a) and Pt-based and Zr-based BMGs (Suppl. Mater., Fig. S2), the evolution in ΔH_{rel} with the number of TCs shows qualitatively the same behaviour as the Pd-based BMG. Comparing all the compositions, the number of thermal cycles to reach the peak of stored energy and the relative energy increase are 45 TCs and 333 J mol^{-1} for the Ti-based BMG, 100 TCs and 208 J mol^{-1} for the tilt-cast Pd-based BMG, 35 TCs and 349 J mol^{-1} for the Pt-based BMG, and 30 TCs and 296 J mol^{-1} for the Zr-based BMG. In each case, following extensive thermal cycling, the stored energy decreases to approximately the value for the as-cast state and further CTC does not have a significant effect on the state of the MG.

The initial state of a BMG of given composition may influence its response to CTC. For the Pd-based BMG, we compare the behaviour of samples prepared by tilt-casting (Fig, 2a) and suction-casting (Fig. S2). The suction-cast rods have a higher initial energy (as-cast ΔH_{rel} = 603 J mol^{-1}, compared to 377 J mol^{-1} for tilt-cast). The peak of stored energy occurs with fewer (75) TCs, and the relative increase in stored energy is less (122 J mol^{-1}).

3.2. Mechanical property changes with thermal cycling

3.2.1. Microhardness

Measurements were carried out on the tilt-cast Pd-based BMG in the as-cast state, after CTC (50, 100, 150, 200 TCs) and after 200 TCs + 2 days relaxation at RT, and on the Ti-based BMG in the as-cast state and after CTC (15, 30, 45 and 60 TCs). For each sample, the microhardness varies from place to place, suggesting a variation of local properties. This is usual for both microhardness and nano-indentation characterization of metallic glasses, and is commonly presented as a cumulative

probability distribution (as in Fig. 3). The cumulative distribution changes with the number of TCs to which the BMG was subjected. For the tilt-cast Pd-based BMG (Fig. 3a), the distribution widens at each end, showing both extensive softening and detectable hardening. In contrast, for the Ti-based BMG (Fig. 3b) there is mostly softening.

The evolutions of the microhardness distributions and of ΔH_{rel} are correlated. For each BMG, as ΔH_{rel} increases, the distribution deviates more from that of the as-cast BMG. As ΔH_{rel} decreases back towards its as-cast value, the distribution also reverts towards that of the as-cast state.

It was proposed that CTC increases heterogeneity in MGs [13,18,19] and that this leads to increased plasticity following CTC (e.g. [13,18]). For MGs, characterization of heterogeneity is difficult [9,40]. The width of the hardness distributions (e.g. in Fig. 3) provides an indirect but quantitative measure. We define the width w as the difference between the 1st and 9th decile, normalized by the median of the distribution [26]. The width (w_{Hv}) of the distributions for the tilt-cast Pd-based BMG evolves with ongoing CTC (Fig. 2b) similarly to the evolution of ΔH_{rel}. The maximum observed reduction in average hardness is ~2%, in good agreement with decreases observed in other MGs [16,20,26].

3.2.2. Resonant ultrasound spectroscopy

A cuboid of the tilt-cast Pd-based BMG was characterized by RUS before and after CTC (up to 100 TCs). The resonant modes in RUS mostly involve shear waves, and accordingly the experimental uncertainty is significantly lower for the shear modulus μ (±0.05 %) than for the bulk modulus B (±3%) [33]. Within the uncertainty, B does not change upon CTC; in contrast, μ progressively decreases up to 100 TCs (Fig. 4). While the decrease in μ is larger than the experimental uncertainty, it is small, at most 0.26% relative to the as-cast state. It is understood that μ is more sensitive than B to changes in structure [41]. Before each RUS spectrum acquisition, the cuboid dimensions were remeasured. Changes were detected just above the resolution of the micrometer (±1 μm). The maximum decrease of the sample density is 0.21(±0.09)% at 100 TCs. Such changes in density are consistent with those measured using gas pycnometry in other CTC studies [16,42]. Values of the inverse of the quality factor, Q^{-1} ($= \frac{\Delta f}{f}$, where Δf is the full width at half maximum height of individual resonance peaks, and f the resonance frequency of the peak), were in the order of 10^{-11}–10^{-12} signifying extremely low acoustic loss. These did not change significantly with the number of thermal cycles.

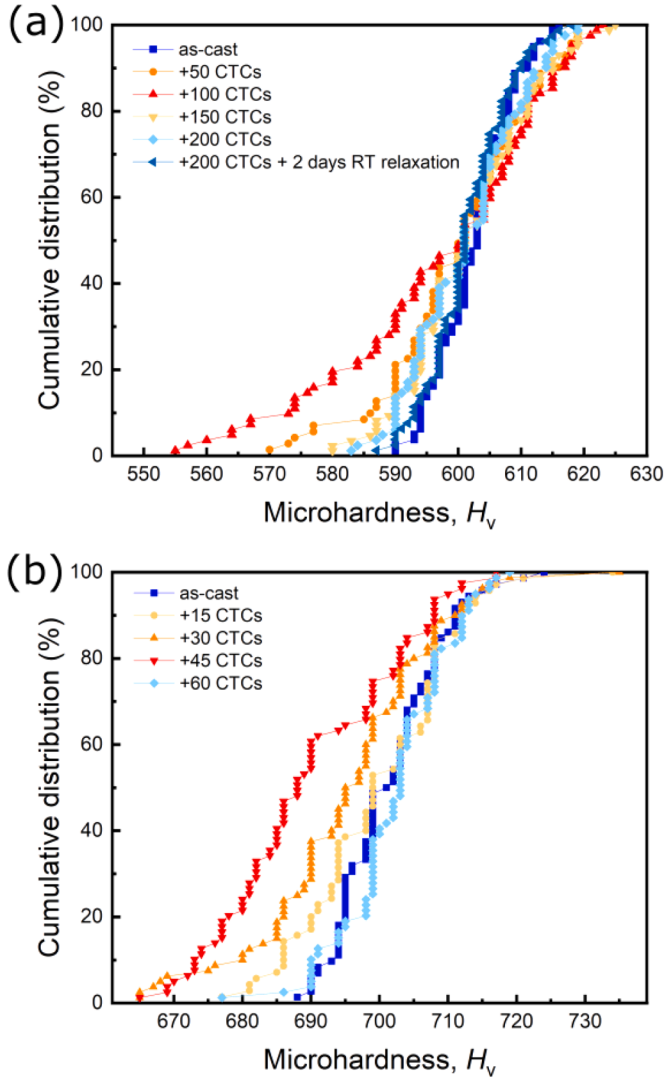

Fig. 3. Evolution of the cumulative distribution of microhardness with CTC for (a) $Pd_{43}Cu_{27}Ni_{10}P_{20}$ (tilt-cast) and (b) $Ti_{40}Zr_{10}Cu_{34}Pd_{14}Sn_2$ BMGs.

3.3. Reversion following rejuvenation

Following CTC, samples were held at RT for various times (t_{hold}) before measuring ΔH_{rel}. Fig. 5a,b shows the evolution of ΔH_{rel} with t_{hold} for the tilt-cast Pd-based BMG after 35, 70 and 100 TCs, and for the Ti-based BMG after 30 TCs. The effects of CTC have a relatively short duration, even at RT. For each treatment, ΔH_{rel} decreases with t_{hold} until, after 10^5–10^6 s, it reaches the value characteristic of the as-cast state. This reversion of ΔH_{rel} upon holding at RT after CTC is confirmed for the suction-cast Pd-based BMG and the Zr-based BMG (Fig. S2).

For the tilt-cast Pd-based BMG samples, it is verified that once the CTC-induced ΔH_{rel} has decayed to the value characteristic of the as-cast state, it then stays at approximately that value, at least up to 10^7 s. A decrease in ΔH_{rel} represents relaxation. For comparison, an as-cast sample was kept at RT for six months (~1.5×10^7 s): no change due to structural relaxation was observed within this time interval. Thus the decays in Fig. 5a,b cannot represent a general structural relaxation; rather, they appear to show a reversion specifically from high-energy states induced by CTC.

The cumulative distribution of microhardness also evolves with t_{hold}, as shown (Fig. 6a) for the tilt-cast Pd-based BMG subjected to 100 TCs (i.e. with the largest hardness change compared to the as-cast state). The effects of CTC are best quantified (§3.2) using the width (w_{Hv}) of the

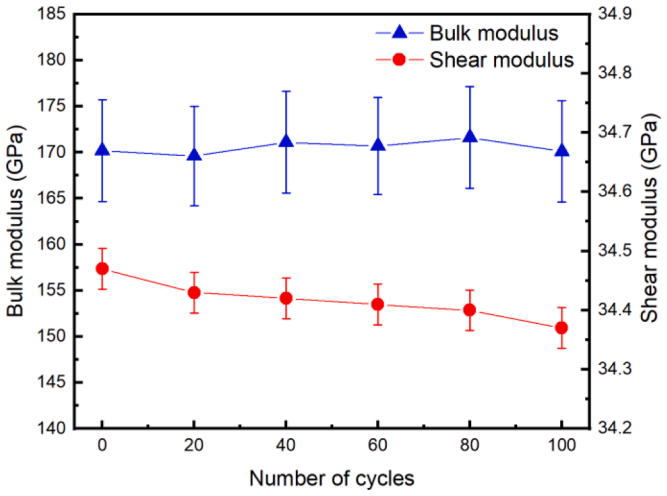

Fig. 4. Shear and bulk moduli derived from resonant ultrasound spectroscopy for a single tilt-cast $Pd_{43}Cu_{27}Ni_{10}P_{20}$ sample in the as-cast state and after treatment up to 100 thermal cycles. While the bulk modulus remains the same within experimental uncertainty, the shear modulus decreases slightly.

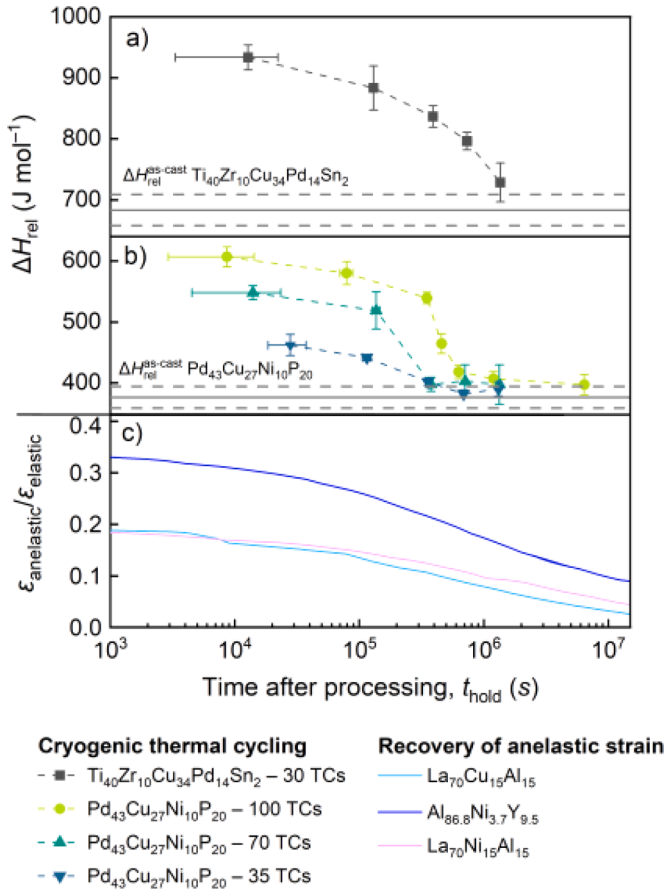

Fig. 5. Decay of ΔH_{rel} with holding time t_{hold} at RT: (a) in $Ti_{40}Zr_{10}Cu_{34}Pd_{14}Sn_2$ BMG after 30 CTCs, and (b) in tilt-cast $Pd_{43}Cu_{27}Ni_{10}P_{20}$ BMG after 35, 70 or 100 CTCs. In (a,b) the solid lines indicate the average ΔH_{rel} of the as-cast state for each composition, and the dashed lines show ±1 SD from the average. (c) The anelastic recovery ($\varepsilon_{anelastic}/\varepsilon_{elastic}$) of three MG compositions following release from deformation around a mandrel (data from [17,43]).

distribution. This increases from 2.3% in the as-cast state to 7.2% when measured soonest (t_{hold} = 24 h) after 100 TCs. With increasing t_{hold}, w_{Hv} decreases, until at 120 h it is approximately the same as for the as-cast state. The decay in w_{Hv} with t_{hold} somewhat precedes the decay of ΔH_{rel} (Fig. 6b).

3.4. Memory effects

With a high number of TCs, samples reach a steady state in which the properties (ΔH_{rel} and cumulative distribution of microhardness) resemble those of the as-cast state. When fewer cycles, giving evident rejuvenation, are followed by sufficient ageing at RT, these properties again resemble those of the as-cast state. We test the similarity of these states (as-cast, steady-state, and aged) that have similar properties.

The as-cast and steady-state MGs, despite having essentially the same calorimetric (Fig. 2a) and mechanical (Figs. 2b and 3) properties, respond differently to CTC. For the as-cast MG, CTC leads to rejuvenation; for the steady-state MG, further CTC has no significant effect on properties. This is a *memory effect*, in which the differing behaviour of two apparently similar samples reveals their differing thermal histories.

Samples of several BMGs were subjected to 200 TCs to attain the steady state in which ΔH_{rel} attains the value characteristic of the as-cast state, and immediate further CTC has no effect. These samples were held at RT long enough (at least 7 days, according to Fig. 5a,b) for near-complete decay of any CTC-induced state. These aged samples were then subjected to a number of TCs and the induced value of ΔH_{rel} was

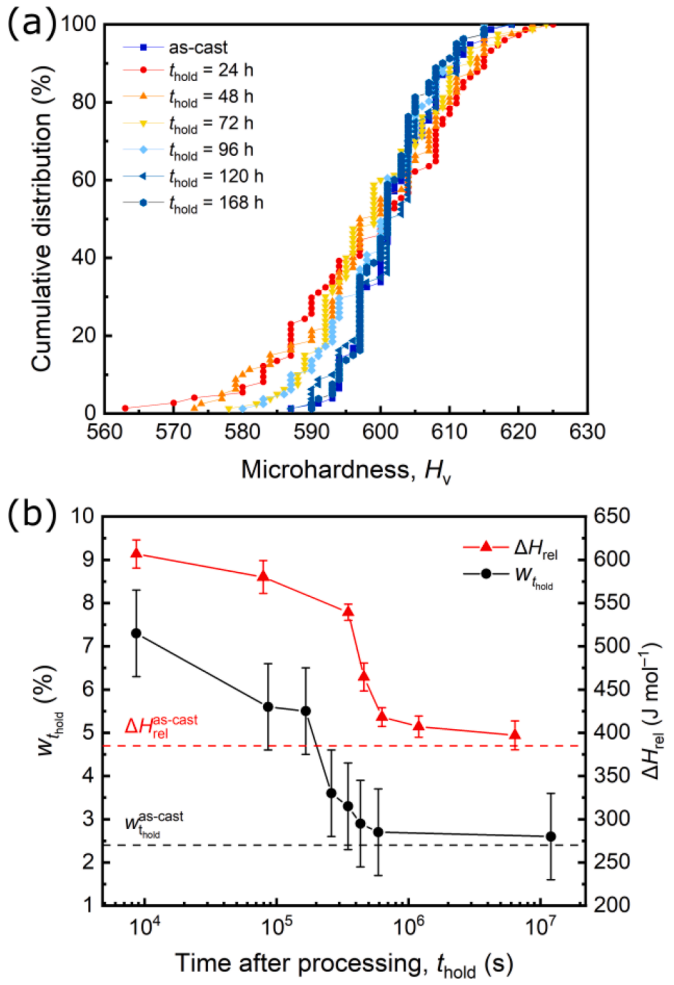

Fig. 6. Property evolution in tilt-cast $Pd_{43}Cu_{27}Ni_{10}P_{20}$ BMG with time elapsed (t_{hold}) following 100 TCs: (a) cumulative distributions of local microhardness; (b) the heat of relaxation ΔH_{rel} evolves similarly to the width w_{Hv} of the cumulative distributions, suggesting that ΔH_{rel} is closely related to the degree of heterogeneity in the glass.

compared with that induced by the same number of TCs applied to the equivalent as-cast glass. In every case, the two values of ΔH_{rel} match within experimental error. This can be seen: for tilt-cast Pd-based BMG samples (Fig. 2a); and for suction-cast Pd-based BMG samples and Zr-based BMG samples (Fig. S2).

The same test was applied to samples initially subjected to fewer TCs and not yet in steady state: tilt-cast Pd-based BMG samples with 100 TCs (i.e. maximum rejuvenation) and Ti-based BMG samples with 30 TCs (i.e. in the middle of Regime I). After subsequent RT ageing to allow ΔH_{rel} to revert to its as-cast value, further CTC induced the same final value of ΔH_{rel} as was obtained by applying the same number of TCs to the as-cast glass (Fig. 2a).

These observations imply a comprehensive memory effect in which samples at all stages of CTC, revert to the behaviour of the as-cast state after sufficient ageing at RT.

4. Discussion

4.1. Heterogeneity of MGs

The effects of CTC on MGs are attributable to heterogeneity in the glassy state (§1). Heterogeneity is apparent from the place-to-place variation in microhardness, quantified as the width w_{Hv} of the cumulative distributions (Figs. 3 and 6a). The microhardness distributions in

the present work are narrower (3–7%) than the distributions of properties at the shorter length-scales probed by nanoindentation or atomic force microscopy [44,45] (12–30%), as would be expected for averaging over a greater volume. Nevertheless, it is remarkable that heterogeneity persists over such a wide range of length-scales.

As probed by the microhardness indents, the plastic-zone radius (r_z) associated with the indents [46,47] is given by:

$$\frac{E}{\sigma_y}\tan\beta = 6(1-\upsilon)\left(\frac{r_z}{a}\right)^3 - 4(1-2\upsilon) \quad (1)$$

where E, σ_y and υ are, respectively, the Young modulus, yield stress and Poisson ratio of the indented material, β is the complement of the semi-angle of the indenter, and a is the half-diameter of the indent. The semi-angle of the Vickers indenter tip is 68°, and values for E, σ_y and υ are taken from references [48–50]. Taking the values of a (~6.2 μm and ~5.8 μm) for the as-cast states of the two BMGs, r_z is ~3.8 μm in the tilt-cast Pd-based BMG and ~3.9 μm in the Ti-based BMG. With plastic zones so large, the measurements are not significantly influenced by any surface effects; the distributions of microhardness values represent heterogeneity through the bulk. As microhardness measurements can be affected by residual stresses, the heterogeneity may reflect variations in structure and residual stress. Heterogeneity and related property changes at the μm length-scale have been reported in other MGs (e.g. [19,51,52]).

These plastic zone sizes are 10^3–10^4 times larger than the presumed diameter of STZs [53]. The heterogeneity of MGs is often considered in terms of a relatively rigid matrix containing a dispersion of *soft spots* within which STZs can be stimulated [26]. CTC can affect the population and nature of the soft spots, while having little or no effect on the matrix [13,26]; CTC can thus have a major effect on some properties and not others. For example, the soft spots affect the initiation of plastic flow, while the matrix predominantly determines the elastic properties. The RUS results (§3.2.2) showing little or no change in elastic moduli upon CTC, support the concept of an unchanged rigid matrix.

A MG sample can be loaded for an extended period at fixed strain well within the elastic limit. The instantaneous strain reduction upon unloading is followed by a time-dependent (*anelastic*) recovery to the initial (zero strain) state [17,35]. According to Argon [54], this behaviour arises from local shear transformations induced by the loading; the STZs are separated by an elastically deformed more rigid matrix that retains the memory of the initial glassy state. Upon unloading, the matrix exerts back-stresses on the STZs, promoting reversion to the initial state.

4.2. Evolution of MG properties with CTC

The present results are consistent with CTC-induced property changes in other families of BMGs [13,18], and show three regimes (Fig. 2). Initially accelerating rejuvenation (Regime I) is expected if the heterogeneity that is the basis of CTC effects is also increased by the CTC. With increasing number of TCs, the effects of CTC are expected to saturate as a steady state is established between rejuvenation and relaxation [11]; instead Regime 2 shows a rapid decrease in ΔH_{rel} and w_{Hv}. The rejuvenated states may relax faster due to increased atomic mobility in the MG [55,56]. For the tilt-cast Pd-based BMG subjected to 100 TCs, ΔH_{rel} reverts to the as-cast value over roughly one week at RT (Fig. 5b). Yet in Regime 2, a similarly complete decay is achieved in 120 mins (60 TCs). This is remarkable, given the relatively high T_g of this MG and that the average sample temperature during the CTC is well below RT. Since thermal relaxation over 120 mins is negligible, even when accelerated by prior CTC, the cycling itself must promote an additional mechanism (§4.5) by which ΔH_{rel} and w_{Hv} revert to values characteristic of the as-cast state.

4.3. Decay of the effects of CTC

Meylan et al. [26] performed CTC on a Fe-based MG and observed significant differences in the mechanical properties measured by nano-indentation. Despite the high T_g of the MG, after three months at RT, its properties had reverted to those of the as-cast state. The present work confirms reversion of properties upon holding at RT, but for the first time characterizes the kinetics. The decay times (for ΔH_{rel} and w_{Hv}) in the present work suggest that the reversion seen by Meylan et al. may have been complete well before the measurement at three months.

The reversion of CTC-induced properties demonstrates a structural memory analogous to that of anelasticity in MGs. Whether achieved by loading in simple compression or tension, or by wrapping a MG ribbon around a mandrel [43,57], anelastic effects are induced by stresses on the sample that are largely uniaxial. There is no such directionality in CTC. Temperature change can, however, induce local deviatoric internal stresses [13,27,28].

In the observed memory effects (§3.4), the rejuvenation induced by CTC is analogous to the accumulation of anelastic strain. The anelastic strain recovery of three MGs ($La_{70}Cu_{15}Al_{15}$ and $La_{70}Ni_{15}Al_{15}$ [17], and $Al_{86.8}Ni_{3.7}Y_{9.5}$ [43]) following wrapping of ribbons around a mandrel is shown in Fig. 5c. The observed anelastic strain recovery ($\varepsilon_{anelastic}$) is normalized by the initial elastic strain ($\varepsilon_{elastic}$). The RT decays of ΔH_{rel} and of ($\varepsilon_{anelastic}/\varepsilon_{elastic}$) show sigmoidal profiles characteristic of a distribution of relaxation times [58]. Considering the differences in compositions and characteristic temperatures, it is surprising that the inflection point of the decay is at a similar time in all cases.

For anelastic creep, Argon and Kuo [58] found that for each MG studied there was a wide spectrum of activation energies, but that the spectra for quite different MGs centred on similar values. They attributed this to an intrinsically similar distribution of free volume in all MGs. Perhaps such considerations apply for the decay curves in Fig. 5. The decay of anelastic strain (Fig. 5c) is much broader than that of ΔH_{rel} (Fig. 5b), reflecting a wider range of relaxation time (more than seven orders of magnitude [57]).

4.4. Stored energy as a result of CTC

At all stages of CTC, subsequent sufficient ageing at RT causes reversion of ΔH_{rel} to the value for the as-cast state. As for anelasticity in MGs, a rigid matrix is the most likely basis of this memory. Because of the heterogeneity of thermal expansion in the MG, local internal stresses arise when the temperature is changed [13,28]. Can the associated elastic energy contribute to the measured ΔH_{rel} increase? The maximum possible elastic strain energy per unit volume under uniaxial loading, is $\sigma_y^2/2E$, where σ_y is the yield stress and E the Young modulus. For the Pd-based MG in the present work, $\sigma_y \approx 1.85$ GPa [48], and $E \approx 97$ GPa (calculated from the bulk and shear moduli of the as-cast state, Fig. 4). The density is 9320 kg m^{-3} [59], and accordingly the molar volume is 8.04×10^{-6} m^3 mol^{-1}. The upper bound on possible elastic strain energy is thereby estimated to be 142 J mol^{-1}. In a sample treated by CTC, not subject to any external stress, the internal stresses form a self-balancing pattern in which the root-mean-square value of principal stress must be well below the peak value. Furthermore, the peak value must be below σ_y (to ensure that the matrix deformation remains elastic). Thus, the actual strain energy must be far lower than the upper bound. Yet even the upper-bound value is significantly less than the maximum increase (208 J mol^{-1}) in the stored energy induced by CTC (100 TCs, Fig. 2a). The strain energy in the matrix in the linear-elastic regime can make only a minor contribution to the stored energy in CTC-treated MG samples.

Anelastic strain in MGs represents a balance between the elastic matrix and soft spots that have undergone shear. If the volume fraction of soft spots exceeds a percolation threshold, the matrix cannot remain fully elastic, and the memory of the unloaded state is lost. As analysed by Argon [54], the critical threshold for the onset of memory loss is

4.5–10.5% volume fraction of transformed matter. For present purposes, we consider the range 5–10%. If the CTC-induced increase in ΔH_{rel} is stored entirely in soft spots, then for the maximum increase of 208 J mol^{-1}, the energy in the soft spots must rise by 2 kJ mol^{-1} if their volume fraction is 10%, by 4 kJ mol^{-1} if it is 5%. These stored-energy increases are 40–80% of the enthalpy of melting ΔH_m (5.0 ± 0.2 kJ mol^{-1} [60]), unusually high for thermomechanical processing, but still below the values reached in irradiated MGs [11]. For melt-spun MG ribbons, the values of ΔH_{rel} are typically 1–1.5 kJ mol^{-1}, although values up to 5.5 kJ mol^{-1} have been reported [11]. Thus, the range of states possible in MGs could reach the inferred value of enthalpy in the soft spots. In the constrained geometry of soft spots, it may be possible to reach states that would be extreme for the uniform bulk MG.

4.5. A model for CTC effects

Temperature change induces a heterogeneous pattern of regions with balancing internal stresses (Fig. 7a,b). Each TC imposes loading and unloading on these regions. We consider each region to contain several soft spots (Fig. 7c). This is consistent with the range of length-scale over which heterogeneity is evident (§4.1).

During a TC, soft spots may shear to-and-fro, but some remain sheared, and accordingly there is a small overall shear of the region (Fig. 7d). With successive TCs, more soft spots are sheared, associated with a larger shear of the region (Fig. 7e). The mechanism by which to-and-fro thermal contraction and expansion lead to increasing local and overall strain is obscure, but such ratcheting is observed in polycrystalline metals, for example giving ongoing shape change with successive thermal cycles [61].

Rejuvenated states have both higher enthalpy, and higher atomic mobility. Previously [11], the higher enthalpy and higher mobility were assumed to be present throughout the MG, leading to a steady state with an enthalpy that, depending on the rejuvenation method and the temperature, can be higher or lower than the initial state. In contrast, we now consider that rejuvenation and increased mobility apply only in the soft spots. In that case, with further cycling, the mobility in some soft spots is eventually so high that they can no longer resist the push-back from the matrix (Fig. 7f). The reversal of the shear in these spots leads to partial elastic recovery of the matrix. This recovery in turn increases the push-back on the remaining sheared soft spots, which progressively revert to an unsheared state (Fig. 7g), possibly explaining the rapid decrease in ΔH_{rel} beyond 100 TCs. Such collapse of transformed states has analogies with dilatation and liquefaction in the flow of granular materials [62] and with avalanches [63].

As further TCs are applied, the soft spots do not resume progressive shear to renew rejuvenation; instead, the enthalpy of the sample stays at its as-cast value. This forces the conclusion that although both increased enthalpy and increased mobility occur in Regime I (Fig. 2a), they are largely decoupled in Regimes II and III. In these regimes, although the enthalpy in the soft spots is lowered to values characteristic of the as-cast state, the atomic mobility within them is not lowered so far. The effect of CTC in enhancing relaxation (§3.3) prevents the accumulation of shear and higher enthalpy upon further CTC. The mobility induced by CTC decays upon holding at RT (Fig. 7h), so the ability to rejuvenate upon CTC is recovered (§3.4).

In Regime III, the glass reverts to ('remembers') the enthalpy, but not the mobility of the as-cast state. After holding at RT, it reverts to both the enthalpy and mobility of the as-cast state. This decoupling, or two-stage memory, may be enabled by the wide range of relaxation time for recovery of anelastic strain in MGs [43].

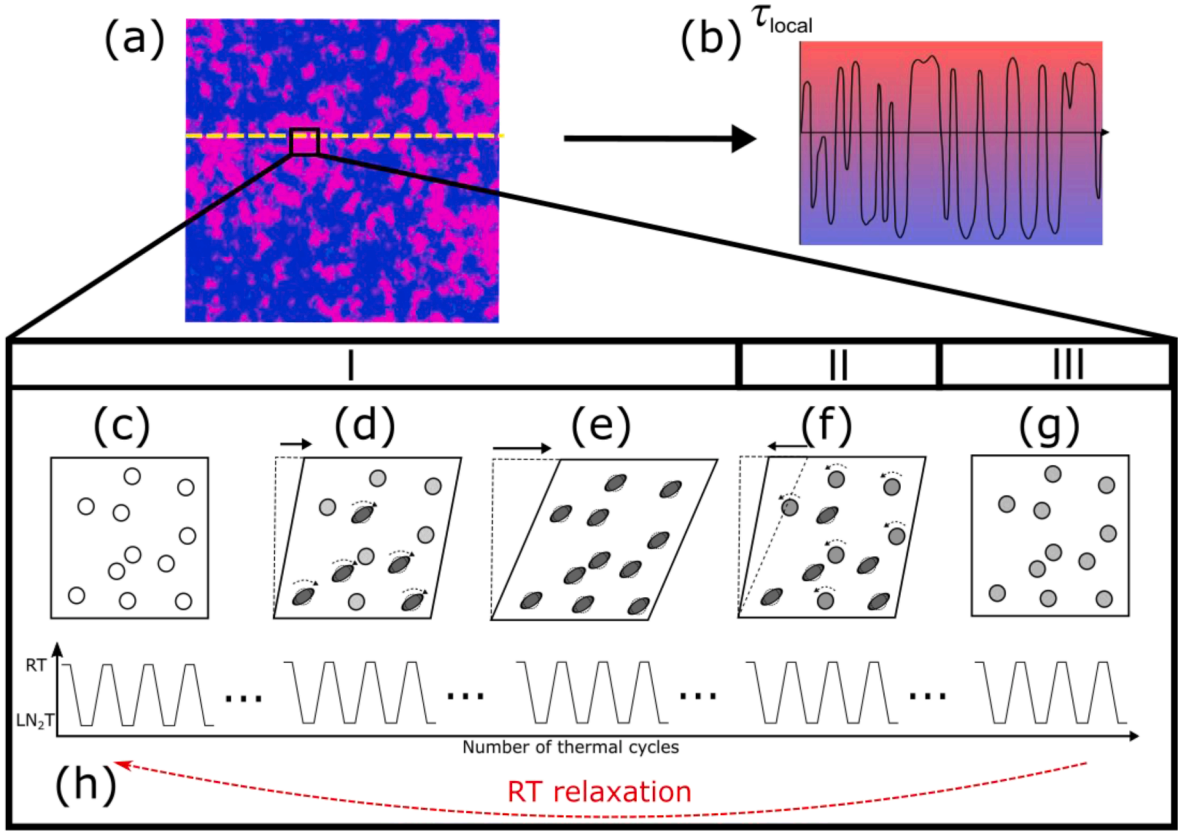

Fig. 7. Schematic model for the structural evolution (Regimes I, II & III) of a MG subjected to an increasing number of TCs. (a) A map of regions within the MG that experience opposing stresses, and (b) a line-scan of opposing shear stresses during thermal cycling. As the cycling continues, initial soft spots (c) within the given region are progressively sheared (d,e). CTC-induced increasing mobility in the soft spots leads to their progressive reversion (f,g) to an unsheared state that retains a higher than initial mobility (indicated by the darker shading). Prolonged holding at RT (h) returns the sample to its as-cast state.

As noted above, it is generally found that the stored energy in a MG first increases and then decreases during progressive CTC. Similar non-monotonic behaviour is not so clear for plasticity, which can continue to rise or saturate [13,19]. The decoupling of enthalpy and mobility may be relevant here: in Regime III, soft spots with CTC-induced higher mobility may maintain increased plasticity, even while the stored energy decreases.

We have not attempted any atomistic modelling of the states depicted in Fig. 7c–g, nor beyond into the aged state (that we take to be identical to the as-cast, Fig. 7c). However, such modelling could provide useful insights into those states, and the transitions between them, as has been shown for a model binary metallic glass subjected to nominally elastic loading and unloading [64]. In that work, local microplastic events occur within an elastic matrix that can exert a back stress. Similar modelling could be particularly useful in understanding Regime II. While in ref. [64], the focus is on thermal activation of the local microplastic events, in Regime II the acceleration of recovery (leading to collapse of the excess enthalpy under applied stress) is attributed to dilatation or other alteration of the soft spots by repeated thermal cycles.

4.6. Implications of anelastic-like effects

If some prominent effects of CTC on MGs are analogous to the accumulation of anelastic strain, that has far-reaching implications—for the interpretation of existing data on CTC effects, and for further research. In the existing literature, the importance of the time elapsed (t_{hold}) between the end of the CTC treatment and the property measurement has not been recognised. With t_{hold} as an uncontrolled variable, results can be scattered, there is a systematic underestimation of the initial effects of CTC, and CTC effects may be missed entirely. The present observations of the transience of CTC effects may, however, help in elucidating the nature of the states induced by CTC, and the mechanisms by which these states are reached.

CTC increases the plasticity and toughness of MGs. Such beneficial effects might also be transitory at RT, but that is not certain as different properties are affected differently. In any case, the effects of CTC can be reinstated at will by treatment after some time at RT: plasticity needed for a deformation or machining process could be reinstated as desired just before that process.

Based on the present work, and considering the apparent universal nature of the three-regime evolution of ΔH_{rel} with CTC in different compositions of MGs (e.g. La-based [13], Ti-based [18], Zr-based [65], Fe-based [66], and Pd-based [22]), we suggest that anelastic-like effects are a universal feature of the rejuvenated states reached by CTC. Such effects may also be relevant for understanding rejuvenation by other techniques involving stimuli within the elastic limit (e.g. elastostatic loading [12] and some mechanical cycling [67]).

5. Conclusion

This work is on four compositions of bulk metallic glass (BMG), based on Pd, Pt, Ti, or Zr. The Pd-based composition is tested in two states, cast at different cooling rates. For all these BMGs, cryogenic thermal cycling (CTC) causes their stored energy to evolve in three regimes: I rejuvenation (increasing enthalpy), II relaxation (decreasing enthalpy), and III steady-state (with enthalpy matching that of the as-cast BMG). The changes in enthalpy are paralleled by changes in the distribution of microhardness values: increased enthalpy correlates with wider distributions indicating increased heterogeneity.

At all stages of processing by CTC (i.e. differing numbers of cycles), its effects are transient: the measured properties revert to those of the as-cast BMG upon holding for roughly one week at RT. This memory of the original state is analogous to that in the anelasticity of MGs. Similar anelastic-like effects may be helpful in understanding rejuvenation by loading (elastostatic or cyclic) within the elastic limit.

We propose that by inducing a pattern of non-affine strains and to-and-fro shear stresses, CTC affects soft spots embedded in a relatively rigid, elastic matrix: the atomic mobility in the soft spots increases, and some of them are sheared. In regime I, soft spots accumulate stored energy through shear. The sheared soft spots impose an increasing retained elastic distortion in the matrix. In regime II, with increased mobility in the soft spots, elastic push-back from the matrix forces a progressive collapse of the CTC-induced shears. In regime III, the CTC-maintained atomic mobility in the soft spots prevents any significant accumulation of shear or stored energy. On holding at RT after cessation of CTC, the mobility relaxes down to values characteristic of the as-cast state.

CTC can induce significant changes in stored energy and hardness distribution in metallic glasses. The memory of the as-cast state implies that the origin of these changes lies in isolated soft spots in which extreme structural and energy states are transiently trapped.

Recognition that the rejuvenation effects of CTC are transient has implications for the interpretation of previously reported results, and for future work on this topic, highlighting that the time elapsed since CTC must be considered for consistent characterization. Although the effects of CTC are transient, they can be renewed at will, and remain relevant for mechanical processing directly after the cycling.

Declaration of Competing Interest

The authors declare that they have no known competing financial interests or personal relationships that could have appeared to influence the work reported in this paper.

Acknowledgements

Support is acknowledged from: the European Union Horizon 2020 Research and Innovation Programme under Marie Skłodowska-Curie grant 861046 (BIOREMIA) for M.B.C. and J.J.L.; the German Research Foundation (DFG) under project GE 1106/15-1 (No. 458057521) for A. G.; the Natural Environment Research Council (grants NE/B505738/1 and NE/F017081/1) and the Engineering & Physical Sciences Research Council (grant EP/I036079/1) for RUS facilities for M.A.C.; and the European Research Council (grant ERC-2015-AdG-695487: ExtendGlass) for A.L.G.

Supplementary materials

Supplementary material associated with this article can be found, in the online version, at doi:10.1016/j.actamat.2022.118551.

References

[1] W.H. Wang, Bulk metallic glasses with functional physical properties, Adv. Mater. 21 (2009) 4524–4544.
[2] C.A. Angell, K.L. Ngai, G.B. McKenna, P.F. McMillan, S.W. Martin, Relaxation in glassforming liquids and amorphous solids, J. Appl. Phys. 88 (2000) 3113–3157.
[3] M. Telford, The case for bulk metallic glass, Mater. Today 7 (2004) 36–43.
[4] J. Schroers, G. Kumar, T.M. Hodges, S. Chan, T.R. Kyriakides, Bulk metallic glasses for biomedical applications, JOM 61 (2009) 21–29.
[5] D.C. Hofmann, L.M. Andersen, J. Kolodziejska, S.N. Roberts, J.-P. Borgonia, W. L. Johnson, K.S. Vecchio, A. Kennett, Optimizing bulk metallic glasses for robust, highly wear-resistant gears, Adv. Eng. Mater. 19 (2017), 1600541.
[6] C.H. Smith, Applications of rapidly solidified soft magnetic alloys, in: H. H. Liebermann (Ed.), Rapidly Solidified Alloys: Processes, Structures, Properties, Applications, Marcel Dekker, New York, 1993, pp. 617–663.
[7] G.D. Herzer, Nanocrystalline soft magnetic materials, Phys. Scr. 1993 (1992) 307–314.
[8] A.L. Greer, Y.Q. Cheng, E. Ma, Shear bands in metallic glasses, Mater. Sci. Eng. R 74 (2013) 71–132.
[9] Y.Q. Cheng, E. Ma, Atomic-level structure and structure-property relationship in metallic glasses, Prog. Mater. Sci. 56 (2011) 379–473.
[10] M.F. Ashby, A.L. Greer, Metallic glasses as structural materials, Scripta Mater. 54 (2006) 321–326.
[11] Y. Sun, A. Concustell, A.L. Greer, Thermomechanical processing of metallic glasses: extending the range of the glassy state, Nat. Rev. Mater. 1 (2016) 16039.
[12] A.L. Greer, Y.H. Sun, Stored energy in metallic glasses due to strains within the elastic limit, Philos. Mag. 96 (2016) 1643–1663.

[13] S.V. Ketov, Y.H. Sun, S. Nachum, Z. Lu, A. Checchi, A.R. Beraldin, H.Y. Bai, W. H. Wang, D.V. Louzguine-Luzgin, M.A. Carpenter, A.L. Greer, Rejuvenation of metallic glasses by non-affine thermal strain, Nature 524 (2015) 200–203.

[14] S.C. Lee, C.M. Lee, J.W. Yang, J.C. Lee, Microstructural evolution of an elastostatically compressed amorphous alloy and its influence on the mechanical properties, Scripta Mater. 58 (2008) 591–594.

[15] H. Zheng, L. Zhu, S.S. Jiang, Y.G. Wang, F.G. Chen, Recovering the bending ductility of the stress-relieved Fe-based amorphous alloy ribbons by cryogenic thermal cycling, J. Alloys Compd. 790 (2019) 529–535.

[16] W. Guo, Y. Shao, M. Zhao, S. Lü, S. Wu, Varying the treating conditions to rejuvenate metallic glass by deep cryogenic cycling treatment, J. Alloys Compd. 819 (2020), 152997.

[17] T.J. Lei, L.R. DaCosta, M. Liu, W.H. Wang, Y.H. Sun, A.L. Greer, M. Atzmon, Microscopic characterization of structural relaxation and cryogenic rejuvenation in metallic glasses, Acta Mater. 164 (2019) 165–170.

[18] J.-L. Gu, H.-W. Luan, S.-F. Zhao, H.-T. Bu, J.-J. Si, Y. Shao, K.-F. Yao, Unique energy-storage behavior related to structural heterogeneity in high-entropy metallic glass, Mater. Sci. Eng. A 786 (2020), 139417.

[19] B.S. Li, S. Xie, J.J. Kruzic, Toughness enhancement and heterogeneous softening of a cryogenically cycled Zr–Cu–Ni–Al–Nb bulk metallic glass, Acta Mater. 176 (2019) 278–288.

[20] W. Guo, R. Yamada, J. Saida, Rejuvenation and plasticization of metallic glass by deep cryogenic cycling treatment, Intermetallics 93 (2018) 141–147.

[21] D. Grell, F. Dabrock, E. Kerscher, Cyclic cryogenic pretreatments influencing the mechanical properties of a bulk glassy Zr-based alloy, Fatigue Fract. Eng. Mater. Struct. 41 (2018) 1330–1343.

[22] J. Ketkaew, R. Yamada, H. Wang, D. Kuldinow, B.S. Schroers, W. Dmowski, T. Egami, J. Schroers, The effect of thermal cycling on the fracture toughness of metallic glasses, Acta Mater. 184 (2020) 100–108.

[23] S.V. Ketov, A.S. Trifonov, Y.P. Ivanov, A.Y. Churyumov, A.V. Lubenchenko, A. A. Batrakov, J. Jiang, D.V. Louzguine-Luzgin, J. Eckert, J. Orava, A.L. Greer, On cryothermal cycling as a method for inducing structural changes in metallic glasses, NPG Asia Mater. 10 (2018) 137–145.

[24] S. Sohrabi, M.C. Ri, H.Y. Jiang, L. Gu, P. Wen, Y.H. Sun, W.H. Wang, Prominent role of chemical heterogeneity on cryogenic rejuvenation and thermomechanical properties of La–Al–Ni metallic glass, Intermetallics 111 (2019), 106497.

[25] S.J. Kang, Q.P. Cao, J. Liu, Y. Tang, X.D. Wang, D.X. Zhang, I.S. Ahn, A. Caron, J. Z. Jiang, Intermediate structural state for maximizing the rejuvenation effect in metallic glass via thermo-cycling treatment, J. Alloys Compd. 795 (2019) 493–500.

[26] C.M. Meylan, F. Papparotto, S. Nachum, J. Orava, M. Miglierini, V. Basykh, J. Ferenc, T. Kulik, A.L. Greer, Stimulation of shear-transformation zones in metallic glasses by cryogenic thermal cycling, J. Non. Cryst. Solids 548 (2020), 120299.

[27] T.C. Hufnagel, Metallic glasses: Cryogenic rejuvenation, Nat. Mater. 14 (2015) 867–868.

[28] B. Shang, P. Guan, J.-L. Barrat, Role of thermal expansion heterogeneity in the cryogenic rejuvenation of metallic glasses, J. Phys. Mater. 1 (2018), 015001.

[29] W. Guo, J. Saida, M. Zhao, S. Lü, S. Wu, Unconspicuous rejuvenation of a Pd-based metallic glass upon deep cryogenic cycling treatment, Mater. Sci. Eng. A 759 (2019) 59–64.

[30] F.O. Méar, B. Lenk, Y. Zhang, A.L. Greer, Structural relaxation in a heavily cold-worked metallic glass, Scripta Mater. 59 (2008) 1243–1246.

[31] A. Bhattacharyya, G. Singh, K.Eswar Prasad, R. Narasimhan, U. Ramamurty, On the strain rate sensitivity of plastic flow in metallic glasses, Mater. Sci. Eng. A 625 (2015) 245–251.

[32] R.E.A. McKnight, M.A. Carpenter, T.W. Darling, A. Buckley, P.A. Taylor, Acoustic dissipation associated with phase transitions in lawsonite, $CaAl_2Si_2O_7(OH)_2{\cdot}H_2O$, Am. Mineral. 92 (2007) 1665–1672.

[33] A. Migliori, J.L. Sarrao, Resonant Ultrasound Spectroscopy: Applications to Physics, Material Measurements and Nondestructive Evaluation, Wiley, New York, 1997.

[34] F.F. Balakirev, S.M. Ennaceur, R.J. Migliori, B. Maiorov, A. Migliori, Resonant ultrasound spectroscopy: The essential toolbox, Rev. Sci. Instrum. 90 (2019), 121401.

[35] A. Concustell, J. Sort, A.L. Greer, M.D. Baró, Anelastic deformation of a $Pd_{40}Cu_{30}Ni_{10}P_{20}$ bulk metallic glass during nanoindentation, Appl. Phys. Lett. 88 (2006), 171911.

[36] A. Migliori, J.D. Maynard, Implementation of a modern resonant ultrasound spectroscopy system for the measurement of the elastic moduli of small solid specimens, Rev. Sci. Instrum. 76 (2005), 121301.

[37] C.T. Moynihan, A.J. Easteal, M.A. Bolt, J. Tucker, Dependence of the fictive temperature of glass on cooling rate, J. Am. Ceram. Soc. 59 (1976) 12–16.

[38] H.B. Yu, W.H. Wang, H.Y. Bai, K. Samwer, The β-relaxation in metallic glasses, Natl. Sci. Rev. 1 (2014) 429–461.

[39] W. Guo, J. Saida, M. Zhao, S. Lü, S. Wu, Rejuvenation of Zr-based bulk metallic glass matrix composite upon deep cryogenic cycling, Mater. Lett. 247 (2019) 135–138.

[40] D.B. Miracle, A structural model for metallic glasses, Nat. Mater. 3 (2004) 697–702.

[41] D. Weaire, M.. Ashby, J. Logan, M.. Weins, On the use of pair potentials to calculate the properties of amorphous metals, Acta Metall. 19 (1971) 779–788.

[42] W. Guo, Y. Shao, J. Saida, M. Zhao, S. Lü, S. Wu, Rejuvenation and plasticization of Zr-based bulk metallic glass with various Ta content upon deep cryogenic cycling, J. Alloys Compd. 795 (2019) 314–318.

[43] J.D. Ju, D. Jang, A. Nwankpa, M. Atzmon, An atomically quantized hierarchy of shear transformation zones in a metallic glass, J. Appl. Phys. 109 (2011), 053522.

[44] D. Tönnies, K. Samwer, P. Derlet, C. Volkert, R. Maaß, Rate-dependent shear-band initiation in a metallic glass, Appl. Phys. Lett. 106 (2015), 171907.

[45] H. Wagner, D. Bedorf, S. Küchemann, M. Schwabe, B. Zhang, W. Arnold, K. Samwer, Local elastic properties of a metallic glass, Nat. Mater. 10 (2011) 439–442.

[46] K.L. Johnson, Contact Mechanics, Cambridge University Press, Cambridge, 1989.

[47] J.J. Kruzic, D.K. Kim, K.J. Koester, R.O. Ritchie, Indentation techniques for evaluating the fracture toughness of biomaterials and hard tissues, J. Mech. Behav. Biomed. Mater. 2 (2009) 384–395.

[48] D. Xing, T. Zhang, W. Li, B. Wei, The characterization of plastic flow in three different bulk metallic glass systems, J. Alloys Compd. 433 (2007) 318–323.

[49] S.L. Zhu, X.M. Wang, A. Inoue, Glass-forming ability and mechanical properties of Ti-based bulk glassy alloys with large diameters of up to 1 cm, Intermetallics 16 (2008) 1031–1035.

[50] P. Gong, L. Deng, J. Jin, S. Wang, X. Wang, K. Yao, Review on the research and development of Ti-based bulk metallic glasses, Metals (Basel) 6 (2016) 264.

[51] K. Nomoto, A.V. Ceguerra, C. Gammer, B. Li, H. Bilal, A. Hohenwarter, B. Gludovatz, J. Eckert, S.P. Ringer, J.J. Kruzic, Medium-range order dictates local hardness in bulk metallic glasses, Mater. Today 44 (2021) 48–57.

[52] C. Liu, R. Maaß, Elastic fluctuations and structural heterogeneities in metallic glasses, Adv. Funct. Mater. 28 (2018), 1800388.

[53] D. Pan, A. Inoue, T. Sakurai, M.W. Chen, Experimental characterization of shear transformation zones for plastic flow of bulk metallic glasses, Proc. Natl. Acad. Sci. U. S. A. 105 (2008) 14769–14772.

[54] A.S. Argon, Mechanisms of inelastic deformation in metallic glasses, J. Phys. Chem. Solids 43 (1982) 945–961.

[55] A.L. Greer, Atomic transport and structural relaxation in metallic glasses, J. Non. Cryst. Solids 61–62 (1984) 737–748.

[56] K. Rätzke, F. Faupel, Diffusion in metallic glasses and undercooled metallic melts, Z. Metallk. 95 (2004) 956–960.

[57] T.J. Lei, L. Rangel DaCosta, M. Liu, W.H. Wang, Y.H. Sun, A.L. Greer, M. Atzmon, Shear transformation zone analysis of anelastic relaxation of a metallic glass reveals distinct properties of α and β relaxations, Phys. Rev. E 100 (2019), 033001.

[58] A.S. Argon, H.Y. Kuo, Free energy spectra for inelastic deformation of five metallic glass alloys, J. Non. Cryst. Solids 37 (1980) 241–266.

[59] L.Y. Watanabe, S.N. Roberts, N. Baca, A. Wiest, S.J. Garrett, R.D. Conner, Fatigue and corrosion of a Pd-based bulk metallic glass in various environments, Mater. Sci. Eng. C 33 (2013) 4021–4025.

[60] G.J. Fan, J.F. Löffler, R.K. Wunderlich, H.J. Fecht, Thermodynamics, enthalpy relaxation and fragility of the bulk metallic glass-forming liquid $Pd_{43}Ni_{10}Cu_{27}P_{20}$, Acta Mater. 52 (2004) 667–674.

[61] K.L. Murty, I. Charit, An Introduction To Nuclear Materials: Fundamentals and Applications, Wiley, New York, 2013, pp. 330–336.

[62] A. Mehta, Granular Physics, Cambridge University Press, Cambridge, 2007.

[63] D. McClung, Snow avalanches as a non-critical, punctuated equilibrium system, in: A.A. Tsonsis, J.B. Elsner (Eds.), Nonlinear Dynamics in Geosciences, Springer, New York, 2007, pp. 429–456.

[64] P.M. Derlet, R. Maaß, Micro-plasticity in a fragile model binary glass, Acta Mater. 209 (2021), 116771.

[65] M. Samavatian, R. Gholamipour, A.A. Amadeh, S. Mirdamadi, Extra rejuvenation of $Zr_{55}Cu_{30}Al_{10}Ni_5$ bulk metallic glass using elastostatic loading and cryothermal treatment interaction, J. Non. Cryst. Solids 506 (2019) 39–45.

[66] H. Zhai, X. Li, W. Li, B. Cheng, D. He, X. Zhang, S. Cui, Strategy for improving the wear-resistance properties of detonation sprayed Fe-based amorphous coatings by cryogenic cycling treatment, Surf. Coatings Technol. 410 (2021), 126962.

[67] P. Ross, S. Küchemann, P.M. Derlet, H. Yu, W. Arnold, P. Liaw, K. Samwer, R. Maaß, Linking macroscopic rejuvenation to nano-elastic fluctuations in a metallic glass, Acta Mater. 138 (2017) 111–118.